Supporting Information

Facile synthesis of Cu/NiCu electrocatalysts integrating alloy, core-shell and one-dimensional structures for efficient methanol oxidation reaction

Dengfeng Wu, Wei Zhang, Daojian Cheng*

Beijing Key Laboratory of Energy Environmental Catalysis, State Key Laboratory of Organic-Inorganic Composites, Beijing University of Chemical Technology, Beijing 100029, China

*E-mail addresses: chengdj@mail.buct.edu.cn

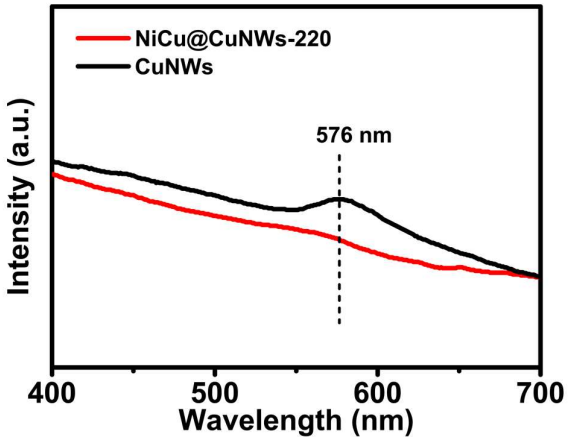

Figure S1. UV-vis spectra of Cu NWs and Cu/NiCu NWs-220.

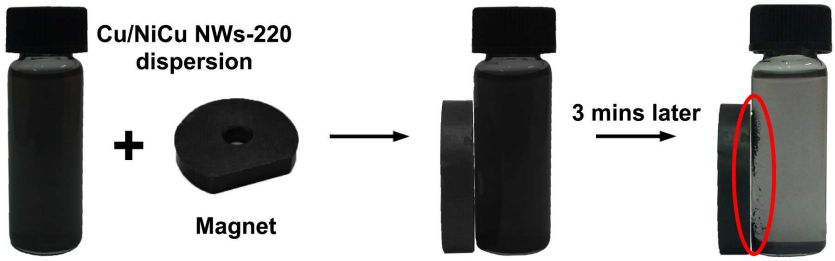

Figure S2. Magnetic response of the Cu/NiCu NWs-220 dispersion to a magnet.

Many previous studies have demonstrated the magnetic properties of NiCu nanoalloys [1-3]. Here, a simple magnetic response test was performed to illustrate magnetic response of Cu/NiCu NWs.

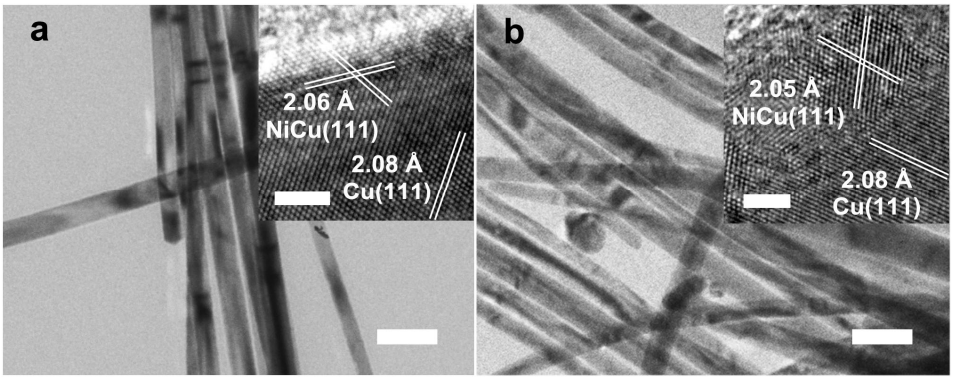

Figure S3. TEM and HRTEM images of (a) Cu/NiCu NWs-210 and (b) Cu/NiCu NWs-230. Scale bars: 50 nm; 2 nm (inserts).

Since the standard interplanar distances of Ni(111) (2.03 Å) and Cu(111) (2.08 Å) are very close, the accuracy of second decimal place at least should be estimated to distinguish different interplanar distances of NiCu(111) in the shell region and Cu(111) in the core region. Here, 10 locations (10 parallel stripes at each location) in core or shell regions were selected and measured to calculate the average value as accurate as possible.

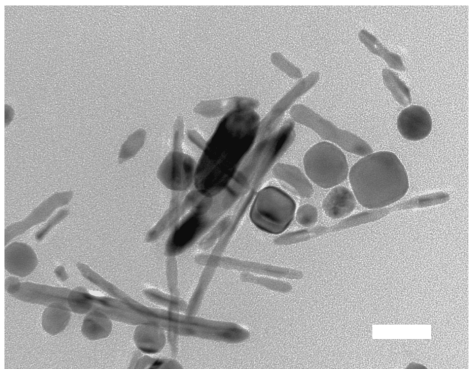

Figure S4. TEM image of NiCu NPs. Scale bar: 50 nm.

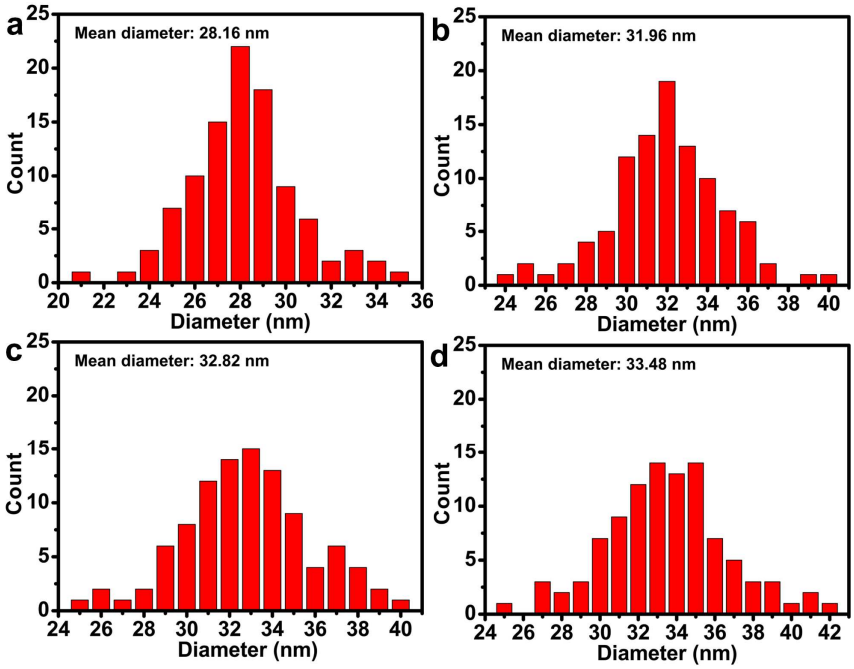

Figure S5. Diameter distribution histograms of (a) Cu NWs, (b) Cu/NiCu NWs-210, (c) Cu/NiCu NWs-220 and (d) Cu/NiCu NWs-230.

The diameter distribution histogram is plotted based on 100 individual nanowires in low magnification image under different view.

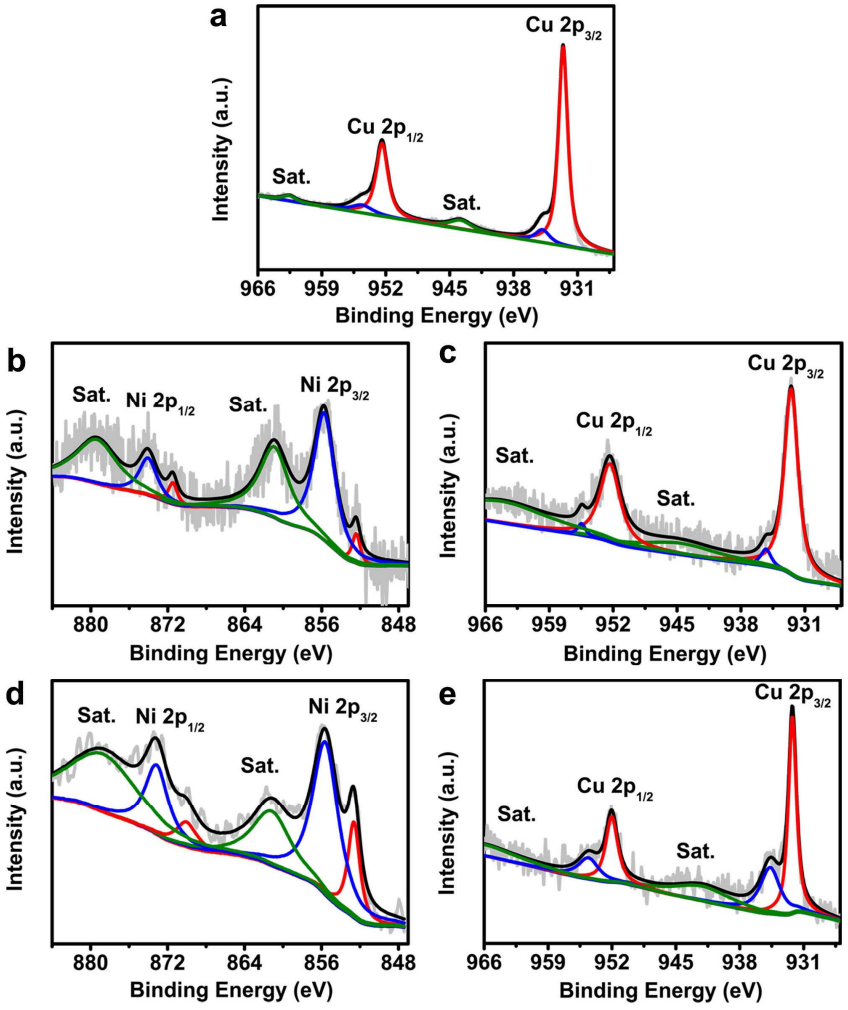

Figure S6. (a) XPS spectra of Ni 2p and Cu 2p in Cu NWs. XPS spectra of Ni 2p and Cu 2p in (b, c) Cu/NiCu NWs-210 and (d, e) Cu/NiCu NWs-230.

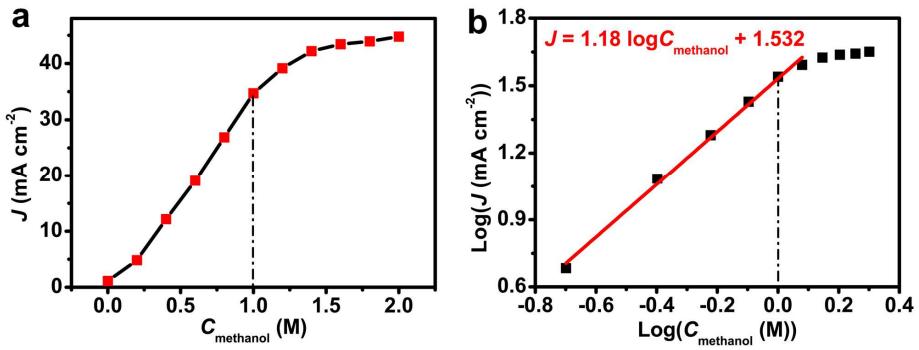

Figure S7. (a) The curve of current densities versus concentrations of methanol on Cu/NiCu NWs-220 electrode at 1.55 V. (b) Fitting of methanol reaction order in methanol oxidation with 1 M KOH.

The logarithmic plot of the current density of MOR on Cu/NiCu NWs-220/C electrode versus the methanol concentration produces a straight line relation (Figure S8b). The slope of the fitting straight line is equal to the order of the MOR as following relations:[4]

$$\log J = \log k + n \log C$$

where J, k, C, n are the peak current density, the reaction rate constant, the concentration of methanol and the reaction order. Value of 1.18 was estimated for the order of MOR at Cu/NiCu NWs-220/C.

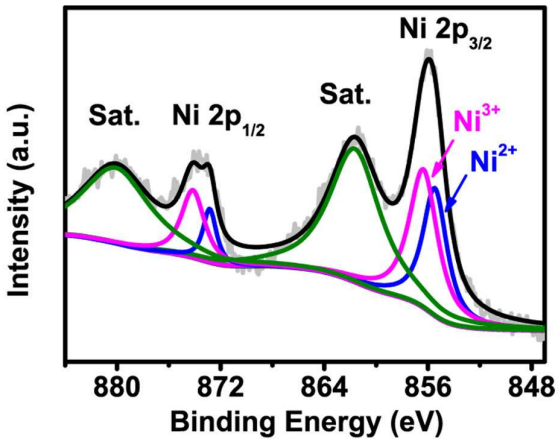

Figure S8. XPS spectra of Ni 2p in Cu/NiCu NWs-220 after CV treatment.

As shown in Figure S8, the fitting peaks around 855.4 eV and 872.8 eV are

indexed to Ni hydroxide, and the fitting peaks at 856.4 eV and 874.1 eV are indexed to Ni nickel oxide hydroxide, which are in accordance to the previous reports.[5-6]

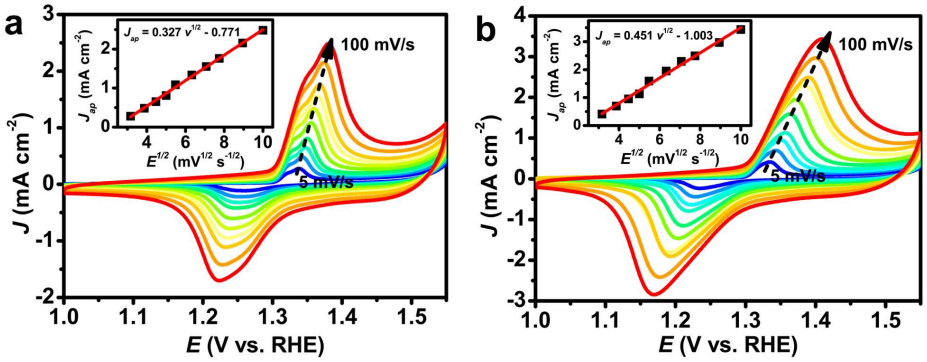

Figure S9. CVs and $J_{ap} \sim v^{1/2}$ relationship of (a) Cu/NiCu NWs-210/C and (b) Cu/NiCu NWs-230/C electrodes in the presence of 1 M KOH at various scan rates of 5, 10, 15, 20, 30, 40, 50, 60, 80 and 100 mV s^{-1}.

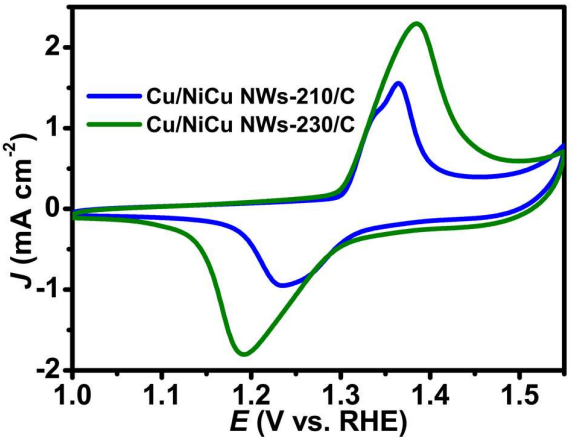

Figure S10. CVs of Cu/NiCu NWs-210/C and Cu/NiCu NWs-230/C electrodes in 1 M KOH with scan rate of 50 mV s^{-1}.

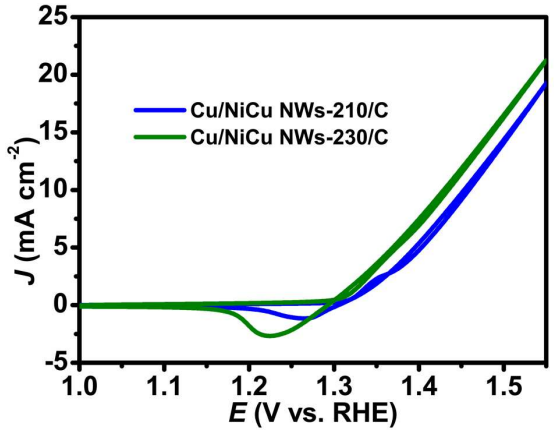

Figure S11. CVs of bare Cu/NiCu NWs-210/C and Cu/NiCu NWs-230/C electrodes in 1 M KOH solution with 1 M methanol at a scan rate of 50 mV s^{-1}.

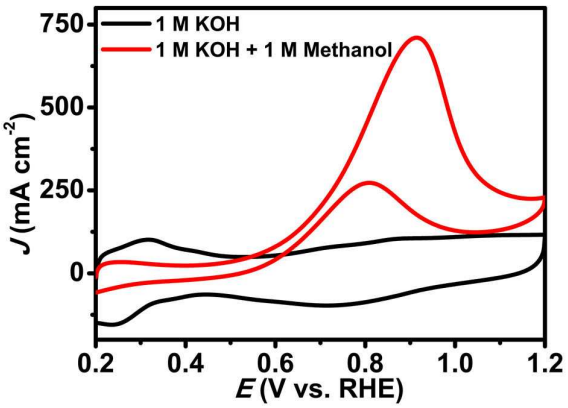

Figure S12. CVs of commercial Pt/C electrodes in 1 M KOH solution with or without 1 M methanol at a scan rate of 50 mV s^{-1}.

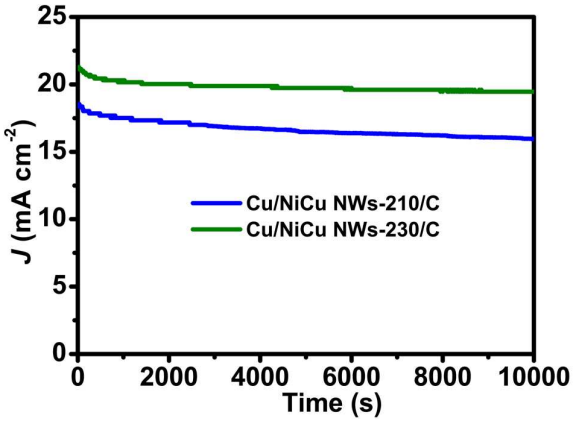

Figure S13. Chronoamperometric responses of Cu/NiCu NWs-210/C and Cu/NiCu NWs-230/C electrodes at 1.55 V (*vs.* RHE) in 1 M KOH electrolyte containing 1 M methanol.

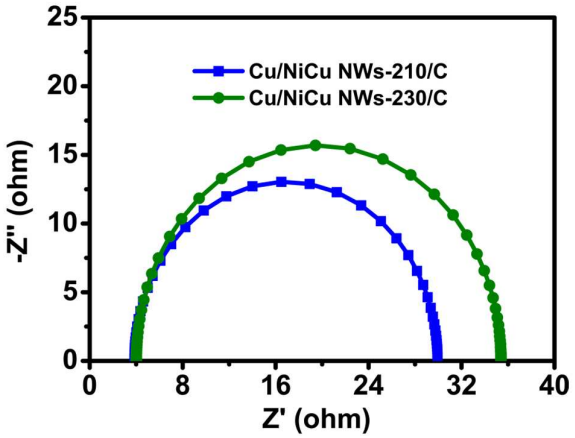

Figure S14. Nyquist plots of Cu/NiCu NWs-210/C and Cu/NiCu NWs-230/C electrodes at 1.4 V (*vs.* RHE) in 1 M KOH electrolyte with 1 M methanol.

Table S1. XRD and XPS data of Cu NWs, Cu/NiCu NWs-210, Cu/NiCu NWs-220 and Cu/NiCu NWs-230.

Samples	XRD	XPS					
	$I_{NiCu(111)}/I_{Cu(111)}$	Ni 2p 3/2 (eV)		Cu 2p 3/2 (eV)		Ni^0:Ni^{2+} (At. %)	Cu:Cu^{2+} (At. %)
		Ni^0	Ni^{2+}	Cu^0	Cu^{2+}		
Cu NWs	--	--	--	932.6	934.9	--	88.9:11.1
Cu/NiCu NWs-210	0.95	852.1	855.0	932.5	934.9	16.9:83.1	91.1:8.9
Cu/NiCu NWs-220	1.25	852.4	855.3	932.3	934.7	18.5:81.5	71.6:28.4
Cu/NiCu NWs-230	1.44	852.6	855.6	932.2	934.6	22.5:77.5	63.3:36.7

Table S2. Atomic Ratio (%) (Cu vs. Ni) of Cu/NiCu NWs-210, Cu/NiCu NWs-220, Cu/NiCu NWs-230, determined by EDX, ICP and XPS analysis.

	Cu/NiCuNWs-210		Cu/NiCuNWs-220		Cu/NiCuNWs-230	
	Cu	Ni	Cu	Ni	Cu	Ni
EDX	93.9	6.1	84.7	15.3	76.1	23.9
ICP	92.6	7.4	83.8	16.2	76.0	24.0
XPS	84.8	15.2	71.5	28.5	58.4	41.6

Reference

(1) Matei, E.; Enculescu, I.; Toimil-Molares, M. E.; Leca, A.; Ghica, C.; Kuncser, V. Magnetic Configurations of Ni–Cu Alloy Nanowires Obtained by the Template Method. *J. Nanopart. Res.* **2013,** *15,* 1863.

(2) Yang, J.; Shen, X.; Ji, Z.; Zhou, H.; Zhu, G.; Chen, K. In Situ Growth of Hollow CuNi Alloy Nanoparticles on Reduced Graphene Oxide Nanosheets and Their Magnetic and Catalytic Properties. *Appl. Surf. Sci.* **2014,** *316,* 575-581.

(3) Baskaran, I.; Sankara Narayanan, T. S. N.; Stephen, A. Pulsed Electrodeposition of Nanocrystalline Cu–Ni Alloy Films and Evaluation of Their Characteristic Properties. *Mater. Lett.* **2006,** *60,* 1990-1995.

(4) Abdel Hameed, R. M.; El-Sherif, R. M. Microwave Irradiated Nickel Nanoparticles on Vulcan XC-72R Carbon Black for Methanol Oxidation Reaction in KOH Solution. *Appl. Catal. B-Environ.* **2015,** *162,* 217-226.

(5) Grosvenor, A. P.; Biesinger, M. C.; Smart, R. S. C.; Mcintyre, N. S. New Interpretations of XPS Spectra of Nickel Metal and Oxides. *Surf. Sci.* **2006,** *600,* 1771-1779.

(6) Casella, I. G.; Guascito, M. R.; Sannazzaro, M. G. Voltammetric and XPS Investigations of Nickel Hydroxide Electrochemically Dispersed on Gold Surface Electrodes. *J. Electroanal. Chem.* **1999,** *462,* 202-210.